Frequency autocorrelation function of stochastically fluctuating fields caused by specific magnetic field inhomogeneities

Cite as: J. Chem. Phys. **129**, 014507 (2008); https://doi.org/10.1063/1.2949097
Submitted: 22 January 2008 . Accepted: 29 May 2008 . Published Online: 02 July 2008

C. H. Ziener, T. Kampf, V. Herold, P. M. Jakob, W. R. Bauer, and W. Nadler

Frequency autocorrelation function of stochastically fluctuating fields caused by specific magnetic field inhomogeneities

C. H. Ziener,[1,a)] T. Kampf,[1] V. Herold,[1] P. M. Jakob,[1,2] W. R. Bauer,[3] and W. Nadler[4]
[1]*Lehrstuhl für Experimentelle Physik 5, Julius-Maximilians-Universität Würzburg, Am Hubland, 97074 Würzburg, Germany*
[2]*Magnetic Resonance Bavaria, Am Hubland, 97074 Würzburg, Germany*
[3]*Medizinische Universitätsklinik, Julius-Maximilians-Universität Würzburg, Josef-Schneider-Strasse 2, 97080 Würzburg, Germany*
[4]*John von Neumann Institute for Computing (NIC), Forschungszentrum Jülich, 52425 Jülich, Germany*

(Received 22 January 2008; accepted 29 May 2008; published online 2 July 2008)

Signal formation in NMR is due to incoherent dephasing of nuclear spins. Of particular practical importance is the situation of nuclear spins undergoing independent stochastic motion in inhomogeneous local magnetic fields, e.g., created by magnetized objects. Since it was demonstrated recently that the frequency correlation function of nuclear spins can be measured directly, a theoretical analysis of such functions is of interest. Here, we provide a numerically exact analysis of that correlation function for the inhomogeneous fields around two particular geometries: cylinders and spheres. The functional form exhibits three regimes: after an initial transient, there is an algebraic regime with a $t^{-d/2}$ time dependence (d being the space dimension), followed by an exponential cutoff due to microscopic system size effects. The main parameter controlling the range of the individual regimes is the volume fraction of the magnetized objects. In addition to our numerical analysis, which is based on eigenfunction expansions, we provide analytical results and approximations based on the generalized moment expansion. © *2008 American Institute of Physics*. [DOI: 10.1063/1.2949097]

I. INTRODUCTION

In magnetic resonance imaging (MRI), the signal from biological tissue is strongly influenced by local inhomogeneous magnetic fields. Of special interest are magnetized objects that are below the spatial resolution of MRI. In biological tissues, these kinds of magnetic field inhomogeneities are generated by deoxygenated red blood cells, capillary networks in the heart or brain, iron-rich cells in the brain, or it is purposefully produced by contrast agents that are used to label cells magnetically. These small magnetic objects create a strongly localized inhomogeneous field at a length scale comparable to the root mean square displacement of a diffusing spin during a MRI experiment. These length scales are typically smaller than a few hundred microns, and diffusion effects can have an important influence on the measured signal. In particular, diffusion can enhance the dephasing of the spins surrounding the magnetic object leading to a faster loss of coherence between them. This loss of coherence has been used in MRI to find relations between the signal intensity and the properties of the magnetic object in question. The increased dephasing can be used to visualize iron oxide labeled cells[1–6] or to study a capillary network[7–12] or lung tissue, where the alveolus is modeled by a sphere surrounded by a water filled shell.[13–16]

The effects of susceptibility inhomogeneities are often described by the transverse relaxation time T_2^*.[17] However, the correct interpretation of T_2^* becomes difficult if the time evolution of the magnetization is not a simple exponential function.[18] In this case, a single parameter will describe the properties of signal formation, and thus the underlying geometry of the magnetic field, only poorly.

Another way to describe the effects of diffusion is in terms of the frequency correlation function $K(t)$, which depends on the probability that a spin transition between two local Larmor frequencies within a specific time.[19] Due to the effects of diffusion, the correlation decreases with time. As it is the case with the MR signal, the frequency correlation function is often assumed to decay exponentially with a characteristic correlation time τ.[20,21] However, in the course of this work, it is shown that this simplification is not valid in all situations.

The relation between the correlation function and relaxation can be seen in the Anderson–Weiss model,[22] which holds when the conditional transition probability between two frequencies is Gaussian.[23] Under this assumption, a relation between the signal intensity and the frequency correlation function[24] can be given as

$$M(t) = \exp\left(- \int_0^t d\xi (t - \xi) K(\xi) \right). \tag{1}$$

Clearly, to study this magnetization time decay, it is necessary to get detailed knowledge about the correlation function $K(t)$. Furthermore, Jensen *et al.*[25] noted that the knowledge of the correct time evolution of the correlation function has a much more direct connection to the local inhomogeneous magnetic field than a simple relaxation rate. They introduced

a)Electronic mail: ziener@physik.uni-wuerzburg.de.

a new method to measure the correlation function directly in a NMR experiment. Another method to analyze the properties of porous media with NMR measurements using the spatial magnetic field correlation function has been reported by Cho and Song.[26] Hence, knowledge about the relationship between generic scenarios of field inhomogeneities and correlation functions is needed to predict the tissue structure from some measured correlation functions.

In the current analysis, we give an overview of the treatment of the correlation function of spins diffusing around a magnetized object. Therefore, after presenting some theoretical basics in Sec. II, restricted and unrestricted diffusion around a spherical and a cylindrical magnetized object is considered in Sec. III. Although the restricted diffusion between two concentric cylinders or spheres has been studied in detail,[27–29] the local magnetic field alters the symmetries of the problem which has to be considered in our analysis. We present closed analytical expressions for the correlation function in this case. The second case we consider is that of unrestricted diffusion, which has already been studied.[30,31] From the analysis of these two cases, it is possible to show that for a certain range of parameters at short and intermediate times, the results of the unrestricted diffusion can be adapted to the restricted case. Thus, it is possible to obtain simple approximations for all time regimes. Furthermore, we analyze the influence of the chosen boundary conditions on the dephasing process.

Additionally, in the case of restricted diffusion, the method of the Padé approximation was used to obtain monoexponential approximations for the correlation function for all time regimes as well as to determine the exponential cutoff. This is done in Sec. IV and can be used to analyze the range of parameters where the choice of boundary conditions influences the diffusion process significantly. The moments obtained from the generalized moment analysis enable us to visualize the Koenig theorem, a very general theorem in the field of operator analysis, which was applied to the diffusion process between two concentric objects. Further, we provide the results for monoexponential decay in the long- and short-time limits of the correlation function. A summary and discussion close this work in Sec. V.

II. GENERAL APPROACH

A. Correlation function

We consider a compact, impermeable magnetized object G in an external magnetic field and observe the trajectory of diffusing spins in a surrounding dephasing volume V where homogeneous diffusion properties are assumed; i.e., inside the dephasing volume V, we neglect the possible diffusion restrictions by membranes or other structures. Due to the presence of the object, the external magnetic field is distorted in its vicinity. This distortion is described by a spatial variation in the Larmor frequency denoted by[32]

$$\omega(\mathbf{r}) = \delta\omega \frac{\partial^2}{\partial z^2} \int_G \frac{d^3\mathbf{r}'}{|\mathbf{r}-\mathbf{r}'|}, \tag{2}$$

where the frequency shift $\delta\omega = \gamma\mu_0 M_0/(4\pi)$ depends on the magnetization difference between the magnetized object and the surrounding medium M_0 only. The integration in Eq. (2) extends over all $\mathbf{r}' \in G$, where G denotes all points inside the magnetized object. The points $\mathbf{r}$ are located in the dephasing volume V only. The diffusion can be described by the stochastic field fluctuations the spin is subjected to. In order to investigate the influence of the fluctuations induced by the field distortion, we start with the two-point correlation function

$$K(t) = \int_V d^3\mathbf{r} \int_V d^3\mathbf{r}_0 \omega(\mathbf{r}) p(\mathbf{r},\mathbf{r}_0,t) p(\mathbf{r}_0)\omega(\mathbf{r}_0), \tag{3}$$

where $p(\mathbf{r},\mathbf{r}_0,t)$ is the probability density of finding a spin at point $\mathbf{r}$ after time t with the initial ($t=0$) position $\mathbf{r}_0$, and $p(\mathbf{r}_0)$ specifies the probability density function of the equilibrium distribution. In our case, the latter is identical to the spin density, which we assume to be homogeneous, i.e.,

$$p(\mathbf{r}_0) = \frac{1}{V}. \tag{4}$$

We assume free diffusion of spins within the dephasing volume; therefore, the probability $p(\mathbf{r},\mathbf{r}_0,t)$ is simply the Green's function of the diffusion equation

$$\frac{\partial}{\partial t} p(\mathbf{r},\mathbf{r}_0,t) = D\Delta p(\mathbf{r},\mathbf{r}_0,t), \tag{5}$$

where D is the diffusion coefficient and Δ denotes the Laplace operator. This directly leads to the expression

$$p(\mathbf{r},\mathbf{r}_0,t) = e^{tD\Delta}\delta(\mathbf{r}-\mathbf{r}_0). \tag{6}$$

Insertion of the probability densities [Eqs. (6) and (4)] into the definition of the correlation function [Eq. (3)] results in

$$K(t) = \frac{1}{V}\int_V d^3\mathbf{r}\,\omega(\mathbf{r}) e^{tD\Delta}\omega(\mathbf{r}). \tag{7}$$

B. Restricted diffusion

The concept of the supply area is often utilized when adapting chemical and physiological problems. This supply area coincides with the dephasing volume V in which the diffusion of the spins occurs. It is particularly useful when a large volume can be split into smaller volumes of similar geometry. For example, in physiology the Krogh capillary model[33] is used to describe myocardial tissue as a single capillary surrounded by a cylindrical dephasing volume.

If the local resonance frequency around the magnetized object is point symmetric, i.e.,

$$\omega(\mathbf{r}) = \omega(-\mathbf{r}), \tag{8}$$

the resonance frequency of the original trajectory at position $-\mathbf{r}$ in the next dephasing volume coincides with the resonance frequency of the reflected particle at position $\mathbf{r}$ in the original dephasing volume. In this work, we analyze the correlation function for the diffusion process around cylinders and spheres, which generate such a point symmetric local resonance frequency. As visualized in Fig. 1, the transition into the next supply volume can be replaced by a reflection on the boundary of the supply area. Therefore, in this model

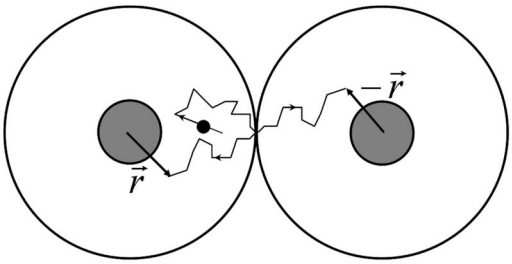

FIG. 1. View of two parallel capillaries (cross section) with supply areas. A sample trajectory of a nuclear spin that leaves the supply area and enters the neighboring supply area is shown. In our model, we replace the original trajectory by a trajectory that is identical to the original one, except that it is reflected at the boundary of the supply area.

a transient trajectory of a particular spin is replaced by a trajectory which is reflected at the boundary.[34] Adapting this model, we assume the reflective boundary conditions at both surfaces.

The diffusion equation (5) can be solved via a spectral expansion

$$p(\mathbf{r},\mathbf{r}_0,t) = \sum_n e^{-Dk_n^2 t}\psi_n(\mathbf{r})\psi_n(\mathbf{r}_0) \tag{9}$$

where the eigenfunctions $\psi_n(\mathbf{r})$ and eigenvalues $-k_n^2$ obey the equation

$$\Delta\psi_n(\mathbf{r}) = -k_n^2\psi_n(\mathbf{r}). \tag{10}$$

In the scope of this work, we consider this equation for cylinders and spheres and will give analytical expressions for the eigenfunctions as well as for the eigenvalues. The spectral expansion [Eq. (9)] of the transition probability $p(\mathbf{r},\mathbf{r}_0,t)$ can be introduced into expression (3). The sum over the eigenvalues in the spectral expansion can be extracted and we obtain, for the correlation function, the sum

$$K(t) = \sum_n \Omega_n^2 e^{-Dk_n^2 t} \tag{11}$$

with the expansion coefficients

$$\Omega_n = \frac{1}{\sqrt{V}}\int_V d^3\mathbf{r}\,\omega(\mathbf{r})\psi_n(\mathbf{r}). \tag{12}$$

In the course of this work, these expansion coefficients Ω_n will be determined for cylindrical and spherical shapes which enable us to calculate the correlation function $K(t)$. Taking into account only the first eigenvalue k_1 in the sum [Eq. (11)], we obtain an expression for the long-time behavior of the correlation function

$$K_c(t) = \Omega_1^2 e^{-Dk_1^2 t}. \tag{13}$$

To consider the initial situation at $t=0$, we use Eq. (6) and find for the initial value of the correlation function

$$K(0) = \langle\omega^2(\mathbf{r})\rangle = \frac{1}{V}\int_V d^3\mathbf{r}\,\omega^2(\mathbf{r}). \tag{14}$$

Asymptotically, the correlation function converges to $K(\infty)=0$. The initial value of the correlation time $K(0)$ can be used to find a connection between the expectation value of the local resonance frequency and the sum over the expansion coefficients, i.e.,

$$\sum_n \Omega_n^2 = \langle\omega^2(\mathbf{r})\rangle. \tag{15}$$

This relation, which is in analogy to Parseval's theorem in Fourier analysis, is important for numerical evaluation. The initial value of the correlation time $K(0)$ is straightforward to determine by integration. It can be used to check if the number of calculated expansion coefficients is sufficient to describe the problem.

C. Unrestricted diffusion

In the case where no outer boundary is present, the dephasing volume extends from the surface of the magnetized object G to infinity. This model can be applied in the case of small volume fractions, i.e., when the influence of the neighboring objects can be neglected. Because this assumption leads to an infinite dephasing volume, it is necessary to express the dephasing volume V in terms of the volume of the magnetized object G and the volume fraction $\eta=G/(G+V)$, i.e.,

$$\frac{1}{V} = \frac{1}{G}\frac{\eta}{1-\eta} \approx \frac{\eta}{G}. \tag{16}$$

The integration in Eqs. (3) and (7) ranges from the surface of the magnetized object G *ad infinitum*. This can be understood in the sense that within the observation time, the influence of the outer boundary is negligible on the diffusion process, i.e., in the case of very small volume fractions η, most of the spins diffusing around the magnetized object do not reach the outer boundary within the measurement time. We will discuss this in the course of this work in detail.

III. SPECIFIC GEOMETRICAL OBJECTS

A. General considerations

In this section, we consider two special shapes of magnetized objects, e.g., cylinders and spheres which can be solved analytically. A sketch of these geometries is visualized in Fig. 2.

To describe the restricted diffusion, we do not consider diffusion in the whole tissue but focus on the dephasing process around a single magnetized object only. In this case, the dephasing volume is the space between the surface of the impermeable object and the surface of the mean relaxation volume. The form of the mean relaxation volume depends on the form of the magnetized object, i.e., in the case of magnetized spheres with radius R_0, the relaxation volume is the space between two concentric spheres with the radii R_0 and R and the volume fraction of material is $\eta=R_0^3/R^3$. Similarly, for cylinders the relaxation volume is the space between two concentric cylinders with radii R_0 and R and volume fraction $\eta=R_0^2/R^2$. The rationale for this restriction and its mathematical implications for evaluation of diffusion have already been discussed in detail.[34,35] Thus, reflective boundary conditions are assumed as[36]

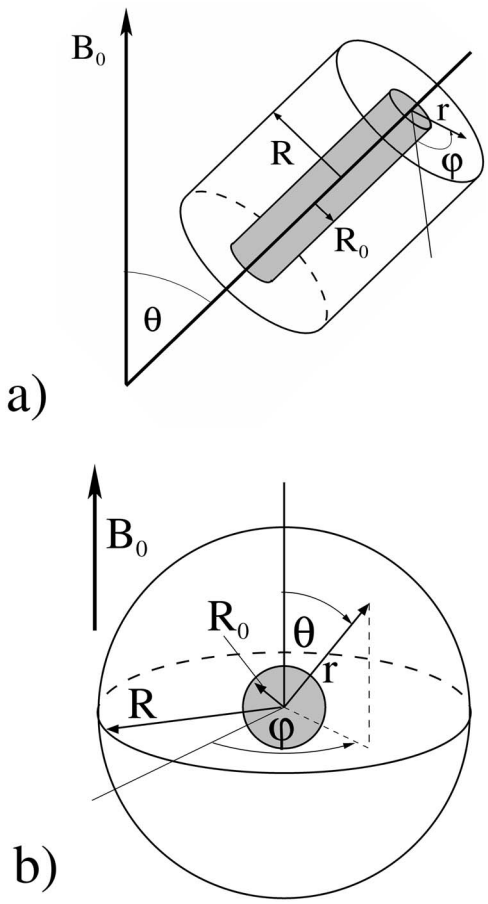

FIG. 2. Scheme of the considered geometries. The dephasing volume is the space between the two concentric cylinders and spheres, respectively. The volume fraction is in the cylindrical case (a) $\eta=R_0^2/R^2$ and in the spherical case (b) $\eta=R_0^3/R^3$. The local frequency around the inner cylinder in (a) is given by Eq. (20), where the two-dimensional polar coordinates (r,φ) are used. In (b) the local frequency around the inner sphere is given by Eq. (34), where the three-dimensional polar coordinates (r,θ,φ) apply. In (a) θ is the angle between the external magnetic field and the axis of the cylinder, while in (b) θ denotes the angle between the external magnetic field and the coordinate vector.

$$\left.\frac{\partial}{\partial r}\right|_{r=R_0} = 0 = \left.\frac{\partial}{\partial r}\right|_{r=R}, \tag{17}$$

where R_0 is the radius of the cylinder or sphere. These relations must be obeyed by any function on which the Laplace operator acts. The radial part of the Laplacian can be cast into a more convenient form

$$\Delta_{d,r} = \frac{1}{r^{d-1}}\frac{d}{dr}r^{d-1}\frac{d}{dr}, \tag{18}$$

where $d=2$ in the case of infinitely long cylinders and $d=3$ in the case of spheres.

The diffusion process is characterized by the correlation time

$$\tau = \frac{R_0^2}{D}. \tag{19}$$

In the case of unrestricted diffusion, the diffusing spins are reflected on the surface of the magnetized object (cylinder or sphere) only. Furthermore, due to the absence of the outer boundary the spins can diffuse to infinity. Thus, only the left hand side of Eq. (17) has to be fulfilled.

Since unrestricted diffusion has been discussed in literature, we only recapitulate these results using our notation and compare it with the results of the restricted diffusion.

B. Cylinders

In the case of cylinders, we have to take into account their orientation to the external magnetic field, as shown in Fig. 2(a). The frequency shift depends on the angle θ between the axis of the cylinder and the direction of the external magnetic field. The local frequency is given by[37]

$$\omega(\mathbf{r}) = \delta\omega R_0^2\frac{\cos 2\varphi}{r^2}, \tag{20}$$

where $\delta\omega$ is the frequency shift on the surface of the cylinder.

1. Restricted diffusion

In the case of restricted diffusion, the transition probability $p(\mathbf{r},\mathbf{r}_0,t)$ has to be evaluated in terms of the spectral expansion [Eq. (9)]. In the two-dimensional case, the solution of the eigenvalue problem [Eq. (10)] is given by the eigenfunctions

$$\psi_n(r,\varphi) = \sum_{\nu=-\infty}^{\infty}[a_{\nu,n}J_\nu(k_n r) + b_{\nu,n}Y_\nu(k_n r)]\frac{e^{i\nu\varphi}}{\sqrt{\pi}}, \tag{21}$$

where J_ν and Y_ν are the Bessel function of the first and second kind, respectively.[38] Introducing these eigenfunctions [Eq. (21)] and the appropriate local resonance frequency from Eq. (20) into the definition of the coefficients Ω_n given in Eq. (12), we can see that only the Bessel functions of the order $\nu=+2$ and $\nu=-2$ are relevant for the eigenfunctions. Using the property of the Bessel function $J_{-2}(x)=J_{+2}(x)$ and $Y_{-2}(x)=Y_{+2}(x)$ and the abbreviations $a_n=a_{+2,n}+a_{-2,n}$ and $b_n=b_{+2,n}+b_{-2,n}$, we finally arrive at

$$\Omega_n = \delta\omega R_0\sqrt{\frac{\eta}{1-\eta}}\int_{R_0}^{R}\frac{dr}{r}[a_n J_2(k_n r) + b_n Y_2(k_n r)]. \tag{22}$$

Thus, we see that only the addend with the index $\nu=2$ in the sum of Eq. (21) contributes to the eigenfunctions, and therefore, the appropriate eigenfunctions in the two-dimensional case can be written in the form

$$\psi_n(r,\varphi) = \frac{1}{\sqrt{\pi}}[a_n J_2(k_n r) + b_n Y_2(k_n r)]\cos 2\varphi. \tag{23}$$

The eigenvalues k_n can be obtained from the reflective boundary conditions at the surface of the inner and outer cylinder. Evaluating the reflective boundary conditions [Eq. (17)], we arrive at an expression for the eigenvalues

$$0 = f(k_n) = J_2'(k_n R_0)Y_2'(k_n R) - J_2'(k_n R)Y_2'(k_n R_0). \tag{24}$$

This equation must be solved numerically to find the appropriate eigenvalues in the spectral expansion. In Fig. 3, the first eigenvalues are visualized in dependence of the volume fraction.

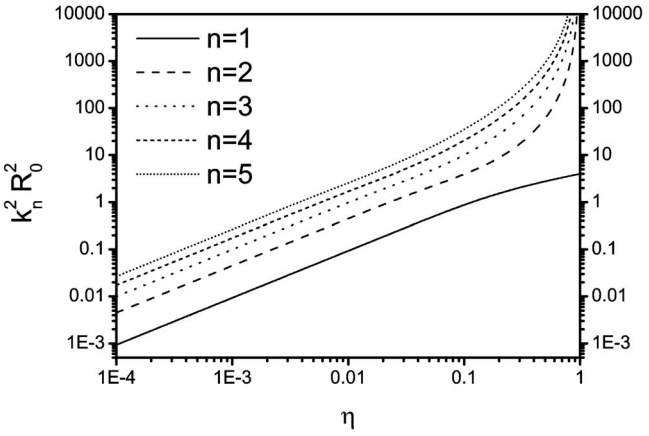

FIG. 3. Eigenvalues for a cylindrical geometry obtained from Eq. (24). For small volume fractions, the eigenvalues can be approximated by the power-law $k_n^2R_0^2=n^2\pi^2\eta$ according to Eq. (A8) for $n>1$, while the first eigenvalue is approximated by $k_1^2R_0^2\approx 6\eta$ for small volume fractions according to Eq. (A4). In the limit $\eta\to 1$, the first eigenvalue [see Eq. (A5)] takes the value $k_1^2R_0^2=4$, while the higher eigenvalues tend to infinity.

A detailed discussion of this eigenvalue equation is given in Appendix A. Since the first eigenvalue governs the long-time behavior of the correlation function according to Eq. (13), we give an approximation for this eigenvalue for small volume fractions, which is derived in Eq. (A4) of Appendix A: $k_1^2\approx 6\eta/R_0^2$.

To determine the coefficients a_n and b_n, we consider the reflective boundary conditions [see Eq. (17)]. It is obvious to choose the parameters $a_n=+Y_2'(k_nR_0)/N_n$ and $b_n=-J_2'(k_nR_0)/N_n$, where N_n is a normalization constant which results from the orthonormality of the eigenfunctions. Introducing these coefficients into the eigenfunction [Eq. (23)], we obtain the expression

$$\psi_n(r,\varphi)=\frac{1}{\sqrt{\pi}N_n}[Y_2'(k_nR_0)J_2(k_nr) - J_2'(k_nR_0)Y_2(k_nr)]\cos 2\varphi. \tag{25}$$

According to standard Sturm–Liouville theory,[39] this normalization constant N_n can be determined using the orthogonality of the eigenfunctions in the interval $R_0\le r\le R$,

$$\int_0^{2\pi} d\varphi \int_{R_0}^{R} drr\psi_n(r,\varphi)\psi_m^*(r,\varphi)=\delta_{nm}, \tag{26}$$

which results in the expression for the normalization constant

$$N_n^2=\int_{R_0}^{R} drr[Y_2'(k_nR_0)J_2(k_nr)-J_2'(k_nR_0)Y_2(k_nr)]^2. \tag{27}$$

To determine the expansion coefficients Ω_n, we introduce the coefficients a_n and b_n into expression (22) and obtain

$$\Omega_n=\frac{\delta\omega R_0}{N_n}\sqrt{\frac{\eta}{1-\eta}}\int_{R_0}^{R}\frac{dr}{r}[Y_2'(k_nR_0)J_2(k_nr) - J_2'(k_nR_0)Y_2(k_nr)]. \tag{28}$$

The integration in Eqs. (27) and (28) is straightforward and we finally arrive at an expression for the expansion coefficient Ω_n^2, which is given in Eq. (B1) of Appendix B. In Fig. 4, the first expansion coefficients are shown as a function of the volume fraction. Using these coefficients Ω_n^2 and the eigenvalues k_n^2, which can be determined from Eq. (24), we can calculate the correlation function $K(t)$ using Eq. (11). In the case of restricted diffusion, the variance of the local magnetic field $\langle\omega^2(\mathbf{r})\rangle=K(0)$ follows from Eq. (14) as

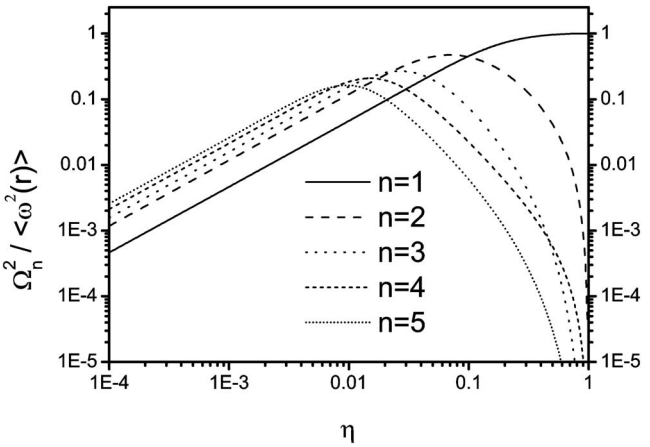

FIG. 4. Coefficients Ω_n^2 for the cylindrical case obtained from Eq. (28). In the limit $\eta\to 1$, only the first coefficient tends to $\Omega_1^2=\langle\omega^2(\mathbf{r})\rangle=\delta\omega^2/2$ given in Eq. (29).

$$\langle\omega^2(\mathbf{r})\rangle=\tfrac{1}{2}\eta\delta\omega^2. \tag{29}$$

In Fig. 5, the correlation function is plotted for different values of the volume fraction η. From this plot, we see that for larger volume fractions, the exponential cutoff starts to approximate the correlation function sufficiently in a shorter period of time than for small volume fractions. Furthermore, for a decreasing volume fraction η, we observe the formation of an intermediate linear regime in the double-logarithmic plot, which corresponds to a power-law decay of the corre-

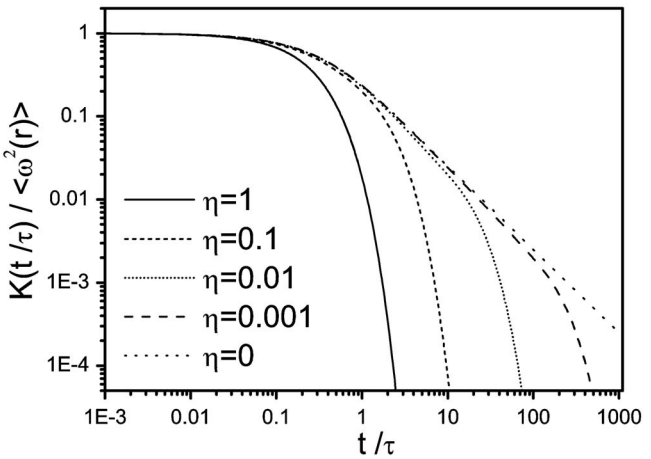

FIG. 5. Correlation function and limiting cases for a cylindrical field inhomogeneity. For restricted diffusion ($\eta=0.1$, $\eta=0.01$, and $\eta=0.001$), the correlation function is obtained from Eq. (11) with initial value from Eq. (29), the coefficients Ω_n^2 given in Eq. (B1) and the eigenvalues k_n^2 as a solution of Eq. (24). According to expression (48), the case of unrestricted diffusion ($\eta=0$) is evaluated via Eq. (30). The limiting case $\eta=1$ is obtained from Eq. (49).

lation function. To analyze this behavior, it is reasonable to consider the case of unrestricted diffusion.

2. Unrestricted diffusion

The case of unrestricted diffusion around a cylinder has been studied in detail by Sukstanskii and Yablonskiy.[30] Thus, in our notation, the following expression for the correlation function takes the form:

$$K_{\mathrm{un}}(t) = \frac{16}{\pi^2}\frac{\eta}{1-\eta}\delta\omega^2\int_0^\infty dx \frac{\exp\left(-\frac{t}{\tau}x^2\right)}{x^5[J_2'^2(x)+Y_2'^2(x)]}. \tag{30}$$

Starting from this result, it is possible to give short- and long-time approximations for the correlation function in the cylindrical case. The short-time approximation for cylinders is given by

$$K_a(t) = \frac{\delta\omega^2}{2}\frac{\eta}{1-\eta}\left(1-4\frac{t}{\tau}\right), \tag{31}$$

and the long-time approximation for cylinders can be expressed as

$$K_b(t) = \frac{\delta\omega^2}{8}\frac{\eta}{1-\eta}\frac{\tau}{t}. \tag{32}$$

In the case of unrestricted diffusion, the variance of the local magnetic field $\langle\omega^2(\mathbf{r})\rangle = K(0)$ follows from Eq. (14) with the dephasing volume from Eq. (16),

$$\langle\omega^2(\mathbf{r})\rangle = \frac{1}{2}\frac{\eta}{1-\eta}\delta\omega^2 \approx \frac{1}{2}\eta\delta\omega^2. \tag{33}$$

As expected, for small volume fractions, this variance coincides with the variance for restricted diffusion [see Eq. (29)].

Due to the supply volume approximation, we consider only a single cylinder with tilt angle θ to the external magnetic field [cf. Fig. 2(a)]. If one considers a network of uniform randomly oriented cylinders, the distribution function for the angle θ is $(\sin\theta)/2$, and therefore, the results given above have to be multiplied by a factor of $\langle\sin^4\theta\rangle = 8/15$, which results from the averaging over all cylinder orientations.

C. Spheres

The inhomogeneous field around a magnetic sphere is that of a magnetic dipole, i.e., in spherical coordinates (r,θ,φ),[40]

$$\omega(\mathbf{r}) = \delta\omega R_0^3\frac{3\cos^2\theta-1}{r^3}, \tag{34}$$

where $\delta\omega$ is the frequency shift on the surface of the sphere. The coordinate system and the dephasing volume are visualized in Fig. 2(b). The z-axis of the coordinate system is parallel to the external magnetic field B_0.

1. Restricted diffusion

In analogy to the eigenfunctions of the two-dimensional case given in Eq. (21), the solution of the eigenvalue problem [Eq. (10)] $\Delta\psi_n(r,\theta,\varphi) = -k_n^2\psi_n(r,\theta,\varphi)$ in three dimensions is given by the eigenfunctions

$$\psi_n(r,\theta,\varphi) = \sum_{l=0}^{\infty}\sum_{m=-l}^{l}[a_{l,n}j_l(k_nr)+b_{l,n}y_l(k_nr)]Y_{lm}(\theta,\varphi), \tag{35}$$

where j_l and y_l are the spherical Bessel functions of the first and second kind, respectively, and Y_{lm} are the spherical harmonics. Introducing the local resonance frequency from Eq. (34) and the eigenfunctions [Eq. (35)] into the definition of the coefficients Ω_n given in Eq. (12), we see that due to the form of the local frequency $\omega(\mathbf{r}) = 4\sqrt{\pi/5}\,\delta\omega Y_{20}(\theta,\varphi)\times(R_0/r)^3$, only the spherical harmonic $Y_{20}(\theta,\varphi) = \sqrt{5/\pi}(3\cos^2\theta-1)/4$ is relevant in our case. Thus, the sum in Eq. (35) reduces to

$$\Omega_n = 2\delta\omega\sqrt{\frac{3}{5}\frac{R_0^3\eta}{1-\eta}}\int_{R_0}^{R}\frac{dr}{r}[a_nj_2(k_nr)+b_ny_2(k_nr)]. \tag{36}$$

Therefore, we obtain in analogy to the two-dimensional eigenfunctions [Eq. (23)] the relevant three-dimensional eigenfunctions

$$\psi_n(r,\theta,\varphi) = [a_nj_2(k_nr)+b_ny_2(k_nr)]Y_{20}(\theta,\varphi). \tag{37}$$

In complete analogy to the cylindrical case, we obtain an expression to determine the eigenvalues k_n,

$$0 = f(k_n) = j_2'(k_nR_0)y_2'(k_nR) - j_2'(k_nR)y_2'(k_nR_0). \tag{38}$$

This equation has the same structure as Eq. (24), except that spherical Bessel functions must be used instead. The dependence of the first eigenvalues on the volume fraction shows the same behavior as in the case of cylinders. A detailed discussion of this eigenvalue equation is given in Appendix A. Since the first eigenvalue governs the long-time behavior of the correlation function according to Eq. (13), we give an approximation for this eigenvalue for small volume fractions, which is derived in Eq. (A16) of Appendix A: $k_1^2 \approx 7\eta^{2/3}/R_0^2$.

In analogy to the cylindrical case, we obtain the normalization constant N_n

$$N_n^2 = \int_{R_0}^{R} dr r^2[y_2'(k_nR_0)j_2(k_nr) - j_2'(k_nR_0)y_2(k_nr)]^2 \tag{39}$$

and the coefficients Ω_n

$$\Omega_n = \frac{2\delta\omega}{N_n}\sqrt{\frac{3}{5}\frac{R_0^3\eta}{1-\eta}}\int_{R_0}^{R}\frac{dr}{r}[y_2'(k_nR_0)j_2(k_nr) - j_2'(k_nR_0)y_2(k_nr)]. \tag{40}$$

The integration in Eqs. (39) and (40) is straightforward and we finally arrive at an expression for the expansion coefficient Ω_n^2 which is given in Eq. (B4) of Appendix B. These coefficients can be used to find the exact form of the correlation function. In the case of restricted diffusion around spheres, the variance of the local magnetic field follows as

$$\langle\omega^2(\mathbf{r})\rangle = \frac{4}{5}\eta\delta\omega^2. \tag{41}$$

The correlation function in the case of spheres exhibits a similar time course as in the cylindrical case. For spheres also the three different decay regimes can be observed.

2. Unrestricted diffusion

The unrestricted diffusion in the dipole field of spherical objects has been treated in detail by Ayant *et al.*[31] Sukstanskii and Yablonskiy[30] obtained an analytical expression for the correlation function,

$$K_{\mathrm{un}}(t) = \frac{4}{5}\frac{\eta}{1-\eta}\delta\omega^2 \sum_{k=1}^{3} A_k e^{t/\tau x_k^2} \tilde{\Phi}\left(-x_k\sqrt{\frac{t}{\tau}}\right), \tag{42}$$

where $\tilde{\Phi}(x)=1-\Phi(x)$ and $\Phi(x)$ is the error function,[41] x_k, $k=1,2,3$, are the roots of the cubic equation $9+9x_k+4x_k^2+x_k^3=0$, and

$$A_k = \frac{x_k(4+x_k)}{9+8x_k+3x_k^2}. \tag{43}$$

An equivalent form of the correlation function has been obtained by Hwang and Freed.[42] Approximate values of the roots x_k and the coefficients A_k are as follows:

$$\begin{aligned} &x_1 \approx -1.783, \quad x_2 = x_3^* \approx -1.108 + 1.954i, \\ &A_1 \approx -0.925, \quad A_2 = A_3^* \approx 0.962 - 0.124i. \end{aligned} \tag{44}$$

Starting from this result, it is possible to give short- and long-time approximations for the correlation function in the spherical case. The short-time approximation for spheres is given by

$$K_a(t) = \frac{4}{5}\frac{\eta}{1-\eta}\delta\omega^2\left(1-9\frac{t}{\tau}\right), \tag{45}$$

and the long-time approximation for spheres yields

$$K_b(t) = \frac{2}{15}\frac{\eta}{1-\eta}\frac{\delta\omega^2}{\sqrt{\pi}}\left(\frac{\tau}{t}\right)^{3/2}. \tag{46}$$

This long-time limit for unrestricted diffusion coincides with the results obtained by Sukstanskii and Yablonskiy[43] and Jensen and Chandra.[19] In the case of unrestricted diffusion, the variance of the local magnetic field $\langle\omega^2(\mathbf{r})\rangle = K(0)$ follows from Eq. (14) with the dephasing volume from Eq. (16),

$$\langle\omega^2(\mathbf{r})\rangle = \frac{4}{5}\frac{\eta}{1-\eta}\delta\omega^2. \tag{47}$$

D. Limiting cases and decay regimes

1. Limiting cases

The limit of small volume fractions ($\eta\to 0$) corresponds to the case of unrestricted diffusion ($R\to\infty$), where no outer boundary is present,

$$\lim_{\eta\to 0} K(t) = K_{\mathrm{un}}(t). \tag{48}$$

From a mathematical point of view, it is interesting to analyze the limit of a vanishing dephasing volume ($R\to R_0$), where the volume fraction tends to one ($\eta\to 1$). The specific characteristic of this limiting case is that all eigenvalues tend to infinity except the first eigenvalue which takes the value $k_1=2/R_0$ for cylinders and $k_1=\sqrt{6}/R_0$ for spheres. This fact is derived in Appendix A and is visualized in Fig. 3 for cylinders. Also, the first expansion coefficient Ω_1^2 takes the value $\Omega_1^2=\langle\omega^2(\mathbf{r})\rangle=\delta\omega^2/2$ in the cylindrical case and $\Omega_1^2=4\delta\omega^2/5$ for the spherical case in this limit, while all other expansion coefficients vanish (for cylinders see Fig. 4). Therefore, the sum in Eq. (11) reduces to the addend $n=1$ and with the variance of the local magnetic field given in Eq. (29) for $d=2$ and Eq. (41) for $d=3$, we obtain

$$\lim_{\eta\to 1} K(t) = \frac{3d-1}{10}\delta\omega^2 e^{-2dt/\tau}. \tag{49}$$

In Fig. 5, the time course of the correlation function and the limiting cases are plotted for different volume fractions η in the cylindrical case. The plot clearly shows the expected behavior for the decreasing of the volume fraction. We see that the correlation functions coincide longer for smaller volume fractions since the influence of the outer boundary is decreased. Also, the formation of an intermediate time regime exhibiting a power law for the time evolution of the correlation function is observed only at small volume fractions. We will discuss this in the next paragraph.

2. Decay regimes

Regarding the formation of a power-law decay for small volume fractions as indicated for $d=2$ in Fig. 5, we use the approximations for short and long times to analyze the different time regimes of the correlation function. Considering Eq. (31) for $d=2$ and Eq. (45) for $d=3$, we obtain for short times ($t/\tau \ll 1$) the expression

$$K_a(t) = \langle\omega^2(\mathbf{r})\rangle\left(1-d^2\frac{t}{\tau}\right), \tag{50}$$

from Eq. (32) for $d=2$ and Eq. (46) for $d=3$, we can find an intermediate regime ($1<t/\tau\ll 1/(R_0^2k_1^2)$)

$$K_b(t) = \frac{\langle\omega^2(\mathbf{r})\rangle}{4(2d-3)\Gamma(d/2)}\left(\frac{\tau}{t}\right)^{d/2}, \tag{51}$$

while for long times ($t/\tau \gg 1/(R_0^2k_1^2)$), we use the previously obtained expression Eq. (13):

$$K_c(t) = \Omega_1^2 \exp\left(-R_0^2k_1^2\frac{t}{\tau}\right). \tag{52}$$

While Eq. (52) is obtained from the eigenfunction with the lowest eigenvalue in the spectral expansion of the restricted case, the approximations [Eqs. (50) and (51)] are obtained from the asymptotic expansions of the unrestricted case. However, for small volume fractions, the differences in $K(0)$ between restricted [Eqs. (29) and (41)] and unrestricted [Eqs. (33) and (47)] diffusion are negligible.

For $d=2$ in Fig. 6, the exact time evolution of the correlation function is compared with the approximations of the several regimes. For short times $t\ll\tau$, the linear decay $K_a(t)$ is a good approximation for the correlation function. To analyze the range of validity for the long-time approximation $K_c(t)$, we consider the exponent $R_0^2k_1^2t/\tau$. To find a criterion for the applicability of the exponential cutoff, we set this exponent to one and find $t/\tau\approx 1/(R_0^2k_1^2)$ for the separation of both approximations.

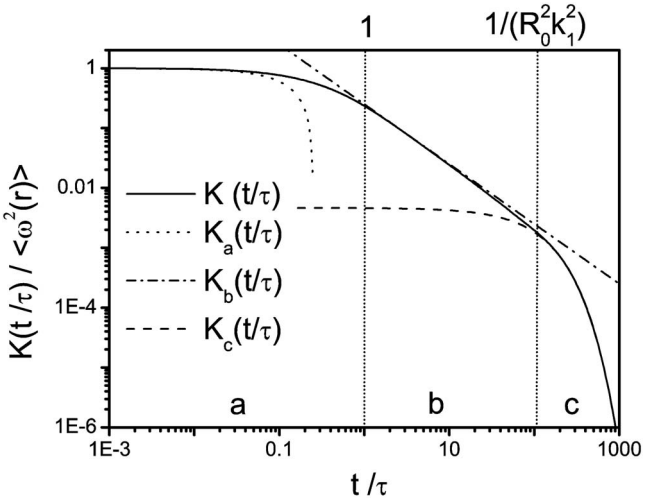

FIG. 6. Regimes for the time evolution of the correlation function for restricted diffusion around a cylinder. The solid line represents the analytical form of the correlation function obtained from Eq. (11) with initial value from Eq. (29) for a volume fraction $\eta=0.001$. The (a) short-, (b) intermediate-, (c) and long-time behaviors are given in Eqs. (50)–(52).

With the approximate first eigenvalue for $d=2$ given in Eq. (A4), we can give a condition which has to be fulfilled to obtain the power-law regime (region b in Fig. 6), i.e., $1/(R_0^2k_1^2)\gg 1$. Finally, we arrived at the condition $\eta\ll(3\sqrt{5}-5)/10\approx 0.17$ for the intermediate regime. If the condition $t/\tau\gg 1/(6\eta)$ is fulfilled, the exponential cutoff $K_c(t)$ given in Eq. (52) can be applied.

In the case of spheres, the approximate first eigenvalue given in Eq. (A16) leads to the condition $\eta\ll 0.05$ for the intermediate regime. The approximation for the exponential cutoff $K_c(t)$ holds for $t/\tau\gg 1/(7\eta^{2/3})$.

To analyze the exponential cutoff in dependence of the dimension, in Fig. 7 we compare the starting point $1/(R_0^2k_1^2)$ of the long-time behavior (region c in Fig. 6) for spheres and cylinders. For a given volume fraction, the exponential cutoff in the three-dimensional case starts at significantly smaller values. The linear segment in the double-logarithmic plot

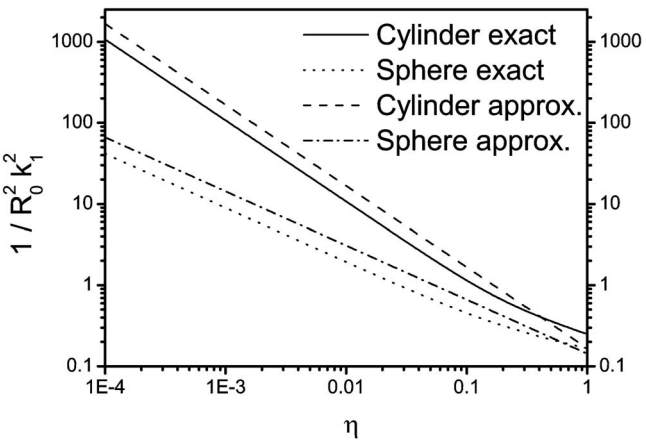

FIG. 7. Starting point $1/(R_0^2k_1^2)$ of the long-time behavior for cylinders and spheres obtained from Eqs. (24) and (38). For small volume fractions, we obtain from Eqs. (A4) and (A16) the approximation $R_0^2k_1^2\approx(4+d)\eta^{2/d}$, which corresponds to the linear regime in the double-logarithmic plot.

reflects the dependence of the first eigenvalue on the volume fraction in form of a power law according to Eqs. (A4) and (A16).

IV. GENERALIZED MOMENT ANALYSIS

A. Monoexponential Padé approximation

The generalized moment expansion method[36,44–47] allows an analytical treatment of the approximate time behavior of $K(t)$. In particular, it provides the possibility of obtaining approximate analytical expressions for the time constant of the exponential cutoff which corresponds to the lowest eigenvalue. In the following, we give a short review of the basic ideas. The starting point of the generalized moment approximation (GMA) is the Laplace transformation of the correlation function [given in Eq. (7)] yielding

$$\hat{K}(s)=\frac{1}{V}\int_V d^3\mathbf{r}\omega(\mathbf{r})\frac{1}{s-D\Delta}\omega(\mathbf{r}). \tag{53}$$

$\hat{K}(s)$ can be expanded in a power series of s for the long-time behavior and in a power series of $1/s$ for the short-time behavior

$$\lim_{s\to 0}\hat{K}(s)=\sum_{n=0}^{\infty}\mu_{-(n+1)}(-s)^n,$$
$$\lim_{s\to\infty}\hat{K}(s)=\frac{1}{s}\sum_{n=0}^{\infty}\mu_n\left(-\frac{1}{s}\right)^n, \tag{54}$$

where the low-frequency moments $\mu_{-(n+1)}$ corresponding to the long-time behavior and high-frequency moments μ_n corresponding to the short-time behavior are given by

$$\mu_{-(n+1)}=\frac{(-1)^n}{n!}\lim_{s\to 0}\frac{d^n\hat{K}(s)}{ds^n}, \tag{55}$$

$$=\frac{1}{n!}\int_0^{\infty}dtt^nK(t), \tag{56}$$

$$\mu_n=\frac{(-1)^n}{n!}\lim_{s\to\infty}\frac{d^n(s\hat{K}(s))}{d\left(\frac{1}{s}\right)^n}, \tag{57}$$

$$=\lim_{t\to 0}\frac{d^nK(t)}{dt^n}. \tag{58}$$

Introducing the correlation function [Eq. (7)] into Eq. (56), for negative n, we obtain

$$\mu_{-n}=\frac{1}{V}\int_V d^3\mathbf{r}\omega(\mathbf{r})[-D\Delta]^{-n}\omega(\mathbf{r}). \tag{59}$$

These moments μ_{-n} depend on the shape of the magnetized object G and the diffusion coefficient D of the surrounding medium only. In view of the expansions (56), we will refer to μ_{-n} as the low-frequency moments. To determine the high-frequency moments μ_n, the correlation function [Eq. (7)] has to be introduced into Eq. (58), e.g., for $n=1$, we obtain

$$\mu_1 = -\frac{D}{V}\int_V d^3\mathbf{r}[\nabla\omega(\mathbf{r})]^2. \tag{60}$$

The general expressions [Eqs. (59) and (60)] obtained above are applied to the two shapes of the magnetized object: cylinders and spheres. For negative n, the moments can be expressed by simple quadratures. Therefore, we write Eq. (59) in the form

$$\mu_{-n} = \frac{1}{VD^n}\int_V d^3\mathbf{r}\,\omega(\mathbf{r})\underbrace{[-\Delta]^{-n}\omega(\mathbf{r})}_{\mu_{-n}(\mathbf{r})}. \tag{61}$$

For this purpose, we define the moment function $\mu_{-n}(\mathbf{r})$ $(n \geq 0)$, which satisfies the equation

$$[-\Delta]^n \mu_{-n}(\mathbf{r}) = \omega(\mathbf{r}). \tag{62}$$

To determine the moments with negative index μ_{-n}, we have to solve this differential equation with the appropriate reflective boundary conditions on the surfaces. The moment μ_0 is identical to the initial value $K(0)$ given in Eq. (14) and has the simple form

$$\mu_0 = \langle\omega^2(\mathbf{r})\rangle. \tag{63}$$

The correlation function $K(t)$ can be approximated by a monoexponential decay in the form

$$K(t) \approx k_{(N_h,N_l)}(t) = f_{(N_h,N_l)}e^{-\Gamma_{(N_h,N_l)}t}, \tag{64}$$

where the prefactor $f_{(N_h,N_l)}$ and the decay constant $\Gamma_{(N_h,N_l)}$ are closely related to the moments μ_n. According to Eq. (53), the Laplace transformation $\hat{K}(s)$ of the correlation function can be approximated by a Lorentzian in the form

$$\hat{K}(s) \approx \hat{k}_{(N_h,N_l)}(s) = \frac{f_{(N_h,N_l)}}{s+\Gamma_{(N_h,N_l)}}, \tag{65}$$

where two parameters have to be determined. This can be done by a $[N_h,N_l]$-Padé approximation, where N_h is the number of high-frequency moments and N_l is the number of low-frequency moments $(N_h+N_l=2)$. The Padé approximant $\hat{k}(s)$ should describe the low-frequency and high-frequency behaviors of Eq. (54) of $\hat{K}(s)$ to a desired degree. We require that $\hat{k}(s)$ reproduces N_h high-frequency and N_l low-frequency moments and refer to the resulting description as the (N_h,N_l)-generalized moment approximation $[(N_h,N_l)$-GMA]. This description represents a two-sided Padé approximation[48,49] around $s=0$ and $s=\infty$.[50] The parameters $f_{(N_h,N_l)}$ and $\Gamma_{(N_h,N_l)}$ are determined by the generalized moments μ_n. For negative index, we introduce Eq. (64) into Eq. (56) and obtain

$$f_{(N_h,N_l)}\Gamma^m_{(N_h,N_l)} = \mu_m,$$

$$m = -N_l, N_h - 1. \tag{66}$$

For positive index $(m \geq 0)$, we introduce Eq. (64) into Eq. (58) and obtain

$$(-1)^m f_{(N_h,N_l)}\Gamma^m_{(N_h,N_l)} = \mu_m,$$

$$m = -N_l, N_h - 1. \tag{67}$$

Knowing the moments μ_n, the solution of Eqs. (66) and (67) provides a monoexponential approximation of the correlation function. The quantities of the left hand side of Eq. (66) or (67) can directly be acquired from the monoexponential approximation of the correlation function according to Eq. (64), while the moments μ_n of the right hand side of Eqs. (66) and (67) are closely related to the shape of the magnetized object as discussed above.

It is worth noting that it is easier to determine the generalized moments μ_n in the case of unrestricted diffusion since the problem could be solved in terms of the Laplace transformation. From Eqs. (55) and (57), it is obvious that the moments μ_n follow from $\hat{K}(s)$ by simple differentiation. However, since asymptotic expansions for the correlation function are available, in this case exploiting the Laplace transformation, the Padé approximant of the correlation function will be calculated in the case of restricted diffusion only.

It is reasonable to define the ratio of successive moments in the form

$$\tau_n = \left|\frac{\mu_n}{\mu_{n+1}}\right|. \tag{68}$$

It can be shown that the series $1/\tau_n$ converges to the lowest eigenvalue of Eq. (10).[35] This follows from Koenig's theorem, a very general result on the zeros of Padé approximants,[51,52] i.e.,

$$k_1^2 = \frac{1}{D}\lim_{n\to\infty}\frac{\mu_{-n}}{\mu_{-(n+1)}}. \tag{69}$$

This first eigenvalue is used in Eq. (13) to describe the long-time behavior of the correlation function. Thus, the statement of Koenig's theorem can be used to determine the first eigenvalue to an arbitrary exactness by using appropriate successive moments. The ratio $\tau_{-1}=\mu_{-1}/\mu_0$, also known as mean relaxation time[53–55] and related to the well-known first passage time, is used quite often as an approximation to the inverse of the first possible eigenvalue.[54] The quantity

$$q_n = |\mu_n\tau_n^n| = \left|\frac{\mu_n^{n+1}}{\mu_{n+1}^n}\right| \tag{70}$$

is the amplitude of the monoexponential decay and therefore an approximation to the contribution of the exponential cutoff of the decay of $K(t)$ if low-frequency moments are used.[35,56]

In the (1,1)-GMA, one low-frequency moment and one high-frequency moment are taken into account, i.e., in Eq. (66) we have $m=-1,0$ and obtain $\Gamma_{(1,1)}=\mu_0/\mu_{-1}=1/\tau_{-1}$ and $f_{(1,1)}=\mu_0=q_{-1}$. From Eq. (56), it is easy to see that the correlation time τ_{-1} can be written in the form

$$\tau_{-1} = \int_0^\infty dt \frac{K(t)}{K(0)} = \int_0^\infty dt t P_c(t). \tag{71}$$

The rate $P_c(t) = -\partial_t K(t)/K(0)$ can be viewed as a "correlation time distribution". We therefore refer to τ_{-1} as the "mean correlation time" and the (1,1)-GMA as the "mean correlation time approximation" (MCTA). MCTA is completely analogous to the "mean relaxation time approximation" in nuclear spin dephasing[57] and analogous to the "mean first passage time approximation" in reaction-diffusion processes.[58] The short-time behavior of the correlation function is approximated by considering the two possible high-frequency moments μ_0 and μ_1. According to Eq. (67), this (2,0)-GMA leads to $\Gamma_{(2,0)} = -\mu_1/\mu_0 = 1/\tau_0$ and $f_{(2,0)} = \mu_0 = q_0$. To describe the correlation function for long times, we take the two possible low-frequency moments μ_{-1} and μ_{-2} into account, i.e., we are in the (0,2)-GMA. From Eq. (66), we have $m = -2, -1$ and obtain $\Gamma_{(0,2)} = \mu_{-1}/\mu_{-2} = 1/\tau_{-2}$ and $f_{(0,2)} = \mu_{-1}^2/\mu_{-2} = q_{-2}$.

It is possible to generalize this result in the case of a monoexponential approximation. Using arbitrary successive moments, we find

$$K_i(t) = q_{-i} e^{-t/\tau_{-i}} = \left| \frac{\mu_{1-i}^i}{\mu_{-i}^{i-1}} \right| e^{-t|\mu_{1-i}/\mu_{-i}|}, \tag{72}$$

with $i \leq 0$ using only high-frequency moments, $i = 1$ using the lowest high-frequency and the lowest low-frequency moment, and $i \geq 2$ using only low-frequency moments. With this, it is possible to adjust the monoexponential approximation to the according time domain of interest. Thus, we can write Koenig's theorem in the form

$$\lim_{i \to \infty} K_i(t) = K_c(t), \tag{73}$$

where the long-time behavior of the correlation function $K_c(t)$ is given in Eq. (13).

B. Cylinders and spheres

To analyze the correlation function of spins diffusing between two concentric cylinders using the GMA, it is necessary to find the moments μ_n as described in Sec. IV A. In order to solve the differential Eq. (62) in the case of cylinders and spheres, the angle dependent part of the local Larmor frequency [Eqs. (20) and (34)] is separated and we use the ansatz

$$\mu_{-n}(\mathbf{r}) = \mu_{-n}(r) \omega(\mathbf{r}) r^d. \tag{74}$$

This leads directly to an iterative set of equations for the functions $\mu_{-n}(r)$

$$\left(\Delta_{d,r} - \frac{2d}{r^2} \right) \mu_{-n}(r) = -\mu_{-(n-1)}(r), \tag{75}$$

which can be solved by

$$\mu_{-n}(r) = \left(\frac{2d}{r^2} - \Delta_{d,r} \right)^{-n} \frac{1}{r^d}. \tag{76}$$

The differential Eq. (75) can be transformed to an Euler differential equation. Using the general expression (74) for the solution of the differential Eq. (62), we find the expression

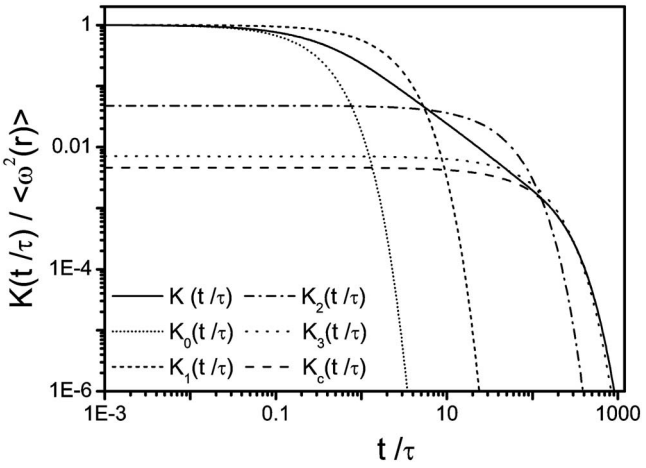

FIG. 8. Monoexponential approximations $K_i(t)$ of the exact correlation function $K(t)$ (solid line) in the cylindrical case for a volume fraction of $\eta = 0.001$. The monoexponential functions $K_i(t)$ are obtained from Eq. (72) using the moments [Eq. (78)]. The long-time approximation $K_c(t)$ (dashed line) is given by Eq. (13) with the first eigenvalue k_1 obtained from Eq. (24).

$$\mu_{-n} = \frac{7d-9}{5} \frac{\delta\omega^2}{D^n} \frac{\eta}{1-\eta} R_0^2 \int_{R_0}^R dr \frac{\mu_{-n}(r)}{r} \tag{77}$$

for the low-frequency moments given in Eq. (59) The evaluation of the integral is straightforward and can be expressed in the general form

$$\mu_n = \frac{\delta\omega^2}{\tau^n} l_n(\eta). \tag{78}$$

For $n = -3, -2, -1, 0, 1$, the results for $l_n(\eta)$ are given in Appendix C. To demonstrate the dependence of the monoexponential approximation on the chosen moments μ_n, different cases are visualized in Fig. 8 for the correlation function around cylinders ($d = 2$). It can clearly be seen that the initial value of $K_i(t), i \geq 1$ decreases with increasing i. The exponential cutoff begins at longer times for increasing i. As expected from Koenig's theorem, the approximants derived by successive moments converge to the long-time approximation given in Eq. (13) obtained by the lowest eigenvalue of Eq. (10).

C. Visualization of Koenig's theorem

Koenig's theorem considers general properties of power series[51] and has applications in the numerical solution of nonlinear equations[52] and the factorization of analytic functions.[59,60] In the situation we deal with here, it states that the ratio of successive moments μ_{-n} converges to the lowest eigenvalue Dk_1^2 [see Eq. (69) above]. The lowest eigenvalue can be obtained exactly by numerically solving the appropriate eigenvalue equation, Eq. (24) for the cylinder and Eq. (38) for the sphere, respectively. Furthermore, a Taylor expansion of these eigenvalue equations is analyzed in Appendix A, yielding the corresponding approximations for the first eigenvalue given in Eqs. (A4) and (A16). In Fig. 9, we demonstrate the predictions of Koenig's theorem and compare them with the Taylor expansion. As expected, for higher

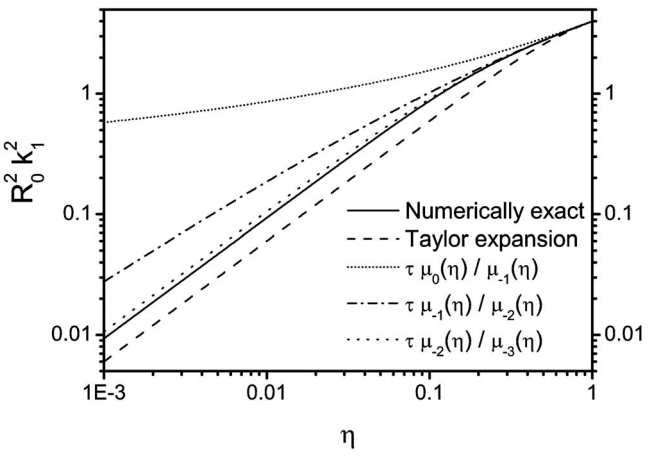

FIG. 9. Dependence of the ratio of successive moments $\tau\mu_{-n}(\eta)/\mu_{-(n+1)}(\eta)=l_{-n}(\eta)/l_{-(n+1)}(\eta)$ on the volume fraction η obtained from Eq. (78) for the cylindrical case. The numerically exact eigenvalue (solid line) can be obtained by solving Eq. (24). The approximant of the first eigenvalue from the Taylor expansion (dashed line) is given in Eq. (A4). For $\eta=1$, all graphs take the value $R_0^2k_1^2=4$ and $\tau\mu_{-n}(1)/\mu_{-(n+1)}(1)=4$.

moments, the approximation converges to the exact first eigenvalue. All ratios of successive moments are larger than the first exact eigenvalue, while the approximate value obtained from the Taylor expansion is smaller. Therefore, these approximants can be used to define a search interval for the numerical solution of Eqs. (24) and (38).

We note that for volume fraction $\eta=1$, all successive moment ratios are identical and equal to the first eigenvalue, i.e.,

$$\tau\frac{\mu_{-n}(\eta=1)}{\mu_{-(n+1)}(\eta=1)}=R_0^2k_1^2(\eta=1)=2d. \tag{79}$$

This simply reflects the fact that in this limit, the frequency correlation function exhibits a monoexponential decay with the respective eigenvalue as time constant.

For small volume fractions η, we observe the opposite behavior. The first ratio—corresponding to the inverse of the normalized mean correlation time $[\tau/\tau_{-1}=\tau\mu_0/\mu_{-1}$, see Eqs. (68) and (71) for their definition]—deviates significantly from the exact lowest eigenvalue according to Eq. (24) and (38). One has to bear in mind that the mean correlation time approximates the time evolution of the correlation function as a monoexponential decay. Since for small volume fraction the formation of a power-law decay is observed at intermediate times (cf. Fig. 5 for the cylindrical case), this deviation reflects the strong nonexponential decay of the frequency correlation function.

V. SUMMARY AND DISCUSSION

Considering the magnetized objects in an external magnetic field, we analyzed the diffusion process of the surrounding spins in terms of the correlation function. In order to perform this analysis, we used an eigenfunction expansion in the case of reflective boundaries and exploited the results of a Laplace analysis in the case of unrestricted diffusion. With these expressions at hand, it is possible to determine the influence of the boundary conditions on the time evolution of the correlation function according to the chosen geometry parameters. If the diffusion is restricted to the space between two concentric objects, the correlation function can, in general, be written as the sum $K(t)=\Sigma_n\Omega_n^2\exp(-Dk_n^2t)$. The expansion coefficients Ω_n and the eigenvalues k_n were studied in detail. The functional form of the correlation function exhibits three different regimes. For each regime, we gave simple approximations for the correlation function as well as the range of their validity. To achieve this, we connected results from the analysis of the unrestricted diffusion for short and intermediate times with the exponential cutoff that appears in the long-time limit as a special feature of the restricted case.

We discussed the influence of the volume fraction η, which—in many applications—is an important parameter that determines the behavior of the system. For small volume fractions, the correlation function of the restricted diffusion process tends to the correlation function of the unrestricted diffusion [see Eq. (48)]. The unrestricted case is applicable to an isolated object and corresponds to an extremely small volume fraction and short times $t\ll\tau$.

Unlike the case of a single magnetized object, the regular arrangement of the capillaries combined with the point symmetry of the frequency $\omega(\mathbf{r})=\omega(-\mathbf{r})$ ensures that the diffusion process is correctly described for larger volume fractions or in the long-time limit. Thus, in our case, the influence of the neighboring objects on the resonance frequency along the trajectory of the spin can be substituted by a reflection at the outer boundary (see Fig. 1).

The limit of a very high volume fraction is more of mathematical interest. In this case, the deviation due to the fact that cylinders and spheres cannot cover a space without overlapping is not negligible. However, from a mathematical point of view, it is interesting that the correlation function shows a monoexponential decay that is governed by the first eigenvalue if the dephasing is restricted to the surface of a cylinder or a sphere.

To validate the results of the eigenfunction expansion, we performed a two-sided Padé approximation and obtained simple expressions for the case of restricted diffusion in the short- and long-time limits. Starting with the Laplace transform of the correlation function, we obtained analytical expressions for the high-frequency and low-frequency moments, respectively. With the help of these moments, we were able to choose the parameters of the Padé approximant to better match the desired properties in the long- or short-time limit. This could be utilized if the underlying problem focuses on very short or very long times to obtain better results.

The low-frequency moments obtained for cylinders and spheres enable us to confirm the well-known Koenig theorem: We could show that the ratio of successive moments converges to the exact first eigenvalue. As expected, for higher volume fraction, the successive moments coincide with the exact first eigenvalue, which reflects the pure monoexponential decay of the correlation function if the diffusion occurs in an infinitely thin shell.

Jensen and Chandra[19] demonstrated that there is a close relationship between the T_2 relaxation time of a Carr–

Purcell–Meiboom–Gill sequence and the correlation function. Thus, knowledge of the correlation function for restricted as well as unrestricted diffusion provides information about sophisticated pulse sequences.

It is worth noting that the monoexponential decay in the (1,1)-GMA is characterized by the time constant $\tau_{-1}=\mu_{-1}/\mu_0$, which coincides with the mean correlation time described in Refs. 8 and 20. When reflective boundary conditions are assumed on both surfaces, the time constant τ_{-1} obtained is the same as the mean correlation time for reflective boundary condition τ_{ref} in Eq. (33) for cylinders and in Eq. (29) for spheres in the work of Ziener *et al.*[20]

It is important to note that the time course of the correlation function depends only on the normalized time t/τ (cf. Fig. 5). This is a general property of the correlation function and coincides with the results in Ref. 61.

ACKNOWLEDGMENTS

This work was supported by the Deutsche Forschungsgemeinschaft—Sonderforschungsbereich 688 "Mechanisms and Imaging of Cell-Cell-Interactions in the Cardiovascular System". Christian H. Ziener thanks the Berufsverband Deutscher Internisten, Wiesbaden, Germany, for providing a scholarship.

APPENDIX A: EIGENVALUES OF THE SPECTRAL EXPANSION

The aim of this appendix is to give some helpful comments to find the eigenvalues k_n of the spectral expansion in the case of restricted diffusion. The eigenvalue equation is obtained from the reflective boundary conditions on the surface of the magnetized object and on the surface of the voxel, i.e.,

$$\left.\frac{\partial}{\partial r}\psi_n(r,\varphi)\right|_{r=R_0}=0=\left.\frac{\partial}{\partial r}\psi_n(r,\varphi)\right|_{r=R}. \tag{A1}$$

This eigenvalue equation can easily be solved numerically using a specialized computer program such as MATHEMATICA® (Wolfram Research, Inc., Champaign, IL).[62]

Nevertheless, it is reasonable to find approximations for these eigenvalues. The long-time behavior of the correlation function is represented by the lowest eigenvalue. Thus, it is helpful to obtain information about this first eigenvalue k_1. There are two possibilities to consider. The first one is a Taylor expansion of the eigenvalue Eq. (A1). The second method to obtain information about the lowest eigenvalue is Koenig's theorem described in Eq. (69), which uses the results of the GMA.

Since there is an infinite number of eigenvalues, numerical evaluation of them is difficult. Hence, for numerical algorithms,[63] it is imperative to use a good initial value for calculating the several eigenvalues. Information about these initial values can be obtained from an asymptotic expansion of the eigenvalue Eq. (A1) for large arguments.

In the case of cylinders, the eigenvalue equation (A1) leads to Eq. (24). The according command in MATHEMATICA® is[64]

$$\{k_1,\ldots,k_n\}=(\mathrm{BesselJPrimeYPrimeJPrimeYPrimeZeros}[2,R/R_0,n])/R_0, \tag{A2}$$

which gives the first n eigenvalues.

For small arguments, the derivatives of the Bessel functions can be written in terms of a Taylor expansion, which enables us to give an approximation of the function $f(k)$ in Eq. (24) for small arguments,

$$f_s(k)\approx\frac{k^2(R^6-R_0^6)+6(R_0^4-R^4)}{3\pi k^2R^3R_0^3}. \tag{A3}$$

Thus, the first zero of the original eigenvalue Eq. (24) can be approximated by the zero of Eq. (A3)

$$k_1^2\approx\frac{6\eta}{R_0^2}\frac{1-\eta^2}{1-\eta^3}\approx\frac{6\eta}{R_0^2}, \tag{A4}$$

which tends for small volume fractions $\eta\to 0$ to $k_1^2\approx 6\eta/R_0^2$. The limiting case $\eta\to 1$ of this first eigenvalue yields

$$\lim_{\eta\to 1}k_1^2(\eta)=\frac{4}{R_0^2}. \tag{A5}$$

This is a specific characteristic of the first eigenvalue since all other eigenvalues tend to infinity in this limit (see Fig. 3). From the well-known large argument asymptotics of the Bessel functions of the first and second kind, an asymptotic expansion of the function $f(k)$ in Eq. (24) leads to an expression for large arguments,

$$f_l(k)\approx\frac{2\sin k(R-R_0)}{k\pi\sqrt{R_0R}}. \tag{A6}$$

The zeros of this asymptotic expansion are the approximate eigenvalues

$$k_n^2\approx\frac{n^2\pi^2}{(R-R_0)^2}=\frac{n^2\pi^2}{R_0^2}\frac{1}{(\eta^{-1/2}-1)^2}. \tag{A7}$$

A Taylor expansion leads to an expression for the eigenvalues for small volume fractions for $n>1$,

$$k_n^2 R_0^2 \approx n^2 \pi^2 \eta. \tag{A8}$$

This power-law dependence corresponds to the linear segment for small volume fractions in Fig. 3.

In the case of spheres, the eigenvalue equation Eq. (A1) leads to Eq. (38). In the current Version 6.0 of MATHEMATICA®, there is no command for spherical Bessel functions equivalent to the command [Eq. (A2)]. Therefore, it is necessary to use the command FindRoot, which requires appropriate boundaries of the search interval. To find these boundaries, an analysis of the spherical eigenvalue equation is performed.

The spherical Bessel functions can be expressed in terms of trigonometric functions. Thus, Eq. (38) can be written in the form

$$k(R_0 - R)A(k,R,R_0)\cos(k(R_0 - R)) = B(k,R,R_0)\sin(k(R_0 - R)) \tag{A9}$$

with the abbreviations

$$A(k,R,R_0) = 4R^2R_0^2k^4 - 9(R^2 - 3R_0R + R_0^2)k^2 + 81,$$

$$B(k,R,R_0) = R^3R_0^3k^6 + RR_0(-9R^2 + 16R_0R - 9R_0^2)k^4 - 9(4R^2 - 9R_0R + 4R_0^2)k^2 + 81.$$

The eigenvalue Eq. (A9) can be written in the form

$$\frac{\tan(k(R_0 - R))}{k(R_0 - R)} = \frac{A(k,R,R_0)}{B(k,R,R_0)}, \tag{A10}$$

which enables us to consider the limiting case $R_0 \to R$ for the left hand side of the equation

$$\lim_{R_0 \to R} \frac{\tan(k(R_0 - R))}{k(R_0 - R)} = \lim_{\eta \to 1} \frac{\tan(k(R_0 - R))}{k(R_0 - R)} = 1 \tag{A11}$$

and the right hand side of the equation

$$\lim_{R_0 \to R} \frac{A(k,R,R_0)}{B(k,R,R_0)} = \lim_{\eta \to 1} \frac{A(k,R,R_0)}{B(k,R,R_0)} \tag{A12}$$

$$= \frac{4R_0^4k^4 + 9R_0^2k^2 + 81}{R_0^6k^6 - 2R_0^4k^4 + 9R_0^2k^2 + 81} = 1. \tag{A13}$$

Equation (A13) can be solved and we finally arrived for this limiting case,

$$\lim_{\eta \to 1} k_1^2(\eta) = \frac{6}{R_0^2}. \tag{A14}$$

For small arguments, the derivatives of the spherical Bessel functions can be written in terms of a Taylor expansion, which enables us to give an approximation of the function $f(k)$ for small arguments,

$$f_s(k) \approx \frac{6}{5}\frac{1}{k^3}\left(\frac{R_0}{R^4} - \frac{R}{R_0^4}\right) + \frac{18(R^7 - R_0^7) + 7R^2R_0^2(R_0^3 - R^3)}{105kR^4R_0^4}. \tag{A15}$$

Thus, the first zero of the original eigenvalue Eq. (38) can be approximated by the zero of Eq. (A15),

$$k_1^2 \approx \frac{1}{R_0^2}\frac{126\eta^{2/3}(1 - \eta^{5/3})}{18 - \eta^{2/3}(7 - 7\eta + 18\eta^{5/3})} \approx \frac{7\eta^{2/3}}{R_0^2}, \tag{A16}$$

which tends for small volume fractions $\eta \ll 0$ to $k_1^2 \approx 7\eta^{3/2}/R_0^2$. In the limit $\eta \to 1$, this eigenvalue tends to $6/R_0^2$, which is in agreement with Eq. (A14).

From the well-known large argument asymptotics of the spherical Bessel functions of the first and second kind, an asymptotic expansion of Eq. (38) leads to an expression for large arguments,

$$f_l(k) \approx \frac{\sin(k(R - R_0))}{k^2RR_0}. \tag{A17}$$

The zeros of this asymptotic expansion are the approximated eigenvalues

$$k_n^2 \approx \frac{n^2\pi^2}{(R - R_0)^2} = \frac{n^2\pi^2}{R_0^2}\frac{1}{(\eta^{-1/3} - 1)^2}. \tag{A18}$$

A Taylor expansion leads to an expression for the eigenvalues for small volume fractions for $n > 1$,

$$k_n^2 R_0^2 \approx n^2\pi^2\eta^{2/3}. \tag{A19}$$

APPENDIX B: ANALYTICAL EXPRESSIONS FOR THE EXPANSION COEFFICIENTS

In this appendix, we present the expression for the expansion coefficient Ω_n^2. In the case of cylinders, we find

$$\Omega_n^2 = \frac{\frac{2\delta\omega^2\eta/(1-\eta)}{J_2'(k_nR_0)Y_2'(k_nR_0)}(Y_2'(k_nR_0)[J_1(k_nR_0) - \sqrt{\eta}J_1(k_nR)] - J_2'(k_nR_0)[Y_1(k_nR_0) - \sqrt{\eta}Y_1(k_nR)])^2}{\frac{Y_2'(k_nR_0)}{J_2'(k_nR_0)}[P(k_nR) - P(k_nR_0)] + \frac{J_2'(k_nR_0)}{Y_2'(k_nR_0)}[Q(k_nR) - Q(k_nR_0)] - \frac{2}{\sqrt{\pi}}[S(k_nR) - S(k_nR_0)]}. \tag{B1}$$

The abbreviations $P(x)$, $Q(x)$, and $S(x)$ are given as

$$P(x) = x^2J_1^2(x) + x^2J_2^2(x) - 4J_1(x)J_2(x),$$

$$Q(x) = x^2 Y_1^2(x) + x^2 Y_2^2(x) - 4 Y_1(x) Y_2(x),$$

$$S(x) = x^2 G_{3,5}^{2,2}\left(x, \tfrac{1}{2} \middle| \begin{matrix} 0, & \tfrac{1}{2}, & -\tfrac{1}{2} \\ 0, & 2, & -2, \quad -1, \quad -\tfrac{1}{2} \end{matrix} \right), \tag{B2}$$

where the Meijer G-function is defined as[65]

$$G_{m,n}^{p,q}\left(z, r \middle| \begin{matrix} a_1, \ldots, a_p \\ b_1, \ldots, b_q \end{matrix} \right) = \frac{1}{2\pi \mathrm{i}} \int_{\gamma_L} ds \frac{\prod_{j=1}^{m} \Gamma(b_j + s) \prod_{j=1}^{n} \Gamma(1 - a_j - s)}{\prod_{j=n+1}^{p} \Gamma(a_j + s) \prod_{j=m+1}^{q} \Gamma(1 - b_j - s)} z^{-s/r} \tag{B3}$$

and the contour γ_L lies between the poles of $\Gamma(1-a_i-s)$ and the poles of $\Gamma(b_i+s)$.

In the case of spheres, the expansion coefficients can be written in the form

$$\Omega_n^2 = \frac{\frac{48\delta\omega^2 \eta/(1-\eta)}{5 j_2'(k_n R_0) y_2'(k_n R_0)} (y_2'(k_n R_0)[\eta T(k_n R) - T(k_n R_0)] - j_2'(k_n R_0)[\eta U(k_n R) - U(k_n R_0)])^2}{\frac{y_2'(k_n R_0)}{j_2'(k_n R_0)}[V(k_n R) - V(k_n R_0)] + \frac{j_2'(k_n R_0)}{y_2'(k_n R_0)}[W(k_n R) - W(k_n R_0)] - 2[X(k_n R) - X(k_n R_0)]}, \tag{B4}$$

with the abbreviations

$$T(x) = x \cos x - \sin x, \quad U(x) = \cos x + x \sin x,$$

$$V(x) = \frac{1}{x^3}[2x^4 - 6(1 + x^2) + 6(1 - x^2)\cos 2x + x(12 - x^2)\sin 2x],$$

$$W(x) = \frac{1}{x^3}[2x^4 - 6(1 + x^2) + 6(x^2 - 1)\cos 2x + x(x^2 - 12)\sin 2x],$$

$$X(x) = \frac{1}{x^3}[x(x^2 - 12)\cos 2x + 6(1 - x^2)\sin 2x]. \tag{B5}$$

APPENDIX C: AUXILIARY FUNCTIONS FOR CALCULATING THE GENERALIZED MOMENTS

In this appendix, we list the functions $l_n(\eta)$ that are necessary to calculate the moments μ_n in Eq. (78). They can be obtained for negative indices from Eq. (77) and the first positive moment is calculated using Eq. (60). In the cylindrical case, the functions are given by

$$l_1(\eta) = -2\eta(1 + \eta), \quad l_0(\eta) = \frac{\eta}{2},$$

$$l_{-1}(\eta) = \frac{1}{8}\frac{\eta \ln \eta}{\eta - 1}, \quad l_{-2}(\eta) = \tfrac{1}{32},$$

$$l_{-3}(\eta) = \frac{1}{256}\frac{\eta}{1 - \eta}\left[\frac{3}{4}\frac{1 - \eta^2}{\eta^2} + \frac{(\ln \eta)^2}{1 - \eta^2}\right]. \tag{C1}$$

In the three-dimensional case, the functions $l_n(\eta)$ can be obtained similarly to the cylindrical case and are given by

$$l_1(\eta) = \frac{36}{5}\eta\frac{1 - \eta^{5/3}}{\eta - 1},$$

$$l_0(\eta) = \tfrac{4}{5}\eta,$$

$$l_{-1}(\eta) = \frac{\eta[32(1 + \eta^{4/3}) + 37(\eta^{1/3} + \eta) + 42a^{2/3}]}{90(\eta^{2/3} + \eta^{1/3} + 1)(\eta^{4/3} + \eta + \eta^{2/3} + \eta^{1/3} + 1)},$$

$$l_{-2}(\eta) = \frac{\eta^{2/3}}{11\,340(\eta^{2/3}+\eta^{1/3}+1)(\eta^{4/3}+\eta+\eta^{2/3}+\eta^{1/3}+1)^2}[972(1+\eta^{8/3})+1684(\eta^{1/3}+\eta^{7/3})+2271(\eta^{2/3}+\eta^2)+2733(\eta+\eta^{5/3})+3580\eta^{4/3}],$$

$$l_{-3}(\eta) = \frac{1}{1\,143\,072(\eta^{2/3}+\eta^{1/3}+1)(\eta^{4/3}+\eta+\eta^{2/3}+\eta^{1/3}+1)^3}[6021(1+\eta^{14/3})+24084(\eta^{1/3}+\eta^{13/3})+47034(\eta^{2/3}+\eta^4)+80260(\eta+\eta^{11/3})+125533(\eta^{4/3}+\eta^{10/3})+180466(\eta^{5/3}+\eta^3)+215176(\eta^2+\eta^{8/3})+230452\eta^{7/3}]. \quad \text{(C2)}$$

[1] T. C. Yeh, W. Zhang, S. T. Ildstad, and C. Ho, Magn. Reson. Med. **30**, 617 (1993).
[2] T. C. Yeh, W. Zhang, S. T. Ildstad, and C. Ho, Magn. Reson. Med. **33**, 200 (1995).
[3] R. Weissleder, H. Cheng, A. Bogdanova, and A. Bogdanova, Jr., J. Magn. Reson Imaging **7**, 258 (1997).
[4] D. L. Kraitchman, A. W. Heldman, E. Atalar, L. C. Ammado, B. J. Martin, M. F. Pittenger, J. M. Hare, and J. W. M. Bulte, Circulation **107**, 2290 (2003).
[5] C. H. Ziener, W. R. Bauer, and P. M. Jakob, Magn. Reson. Med. **54**, 702 (2005).
[6] G. Stoll and M. Bendszus, Stroke **37**, 1923 (2006).
[7] V. G. Kiselev and S. Posse, Phys. Rev. Lett. **81**, 5696 (1998).
[8] W. R. Bauer, W. Nadler, M. Bock, L. R. Schad, C. Wacker, A. Hartlep, and G. Ertl, Magn. Reson. Med. **41**, 51 (1999).
[9] W. R. Bauer, W. Nadler, M. Bock, L. R. Schad, C. Wacker, A. Hartlep, and G. Ertl, Phys. Rev. Lett. **83**, 4215 (1999).
[10] W. R. Bauer, W. Nadler, M. Bock, L. R. Schad, C. Wacker, A. Hartlep, and G. Ertl, Magn. Reson. Med. **42**, 1004 (1999).
[11] W. R. Bauer and W. Nadler, Phys. Rev. E **65**, 066123 (2002).
[12] C. H. Ziener, W. R. Bauer, and P. M. Jakob, Magn. Reson. Mater. Phys., Biol., Med. **18**, 225 (2005).
[13] T. A. Case, C. H. Durney, D. C. Ailion, A. G. Cutillo, and A. H. Morris, J. Magn. Reson. (1969-1992) **73**, 304 (1987).
[14] C. H. Durney, J. Bertolina, D. C. Ailion, R. Christman, A. G. Cutillo, A. H. Morris, and S. Hashemi, J. Magn. Reson. (1969-1992) **85**, 554 (1989).
[15] J. A. Bertolina, C. H. Durney, D. C. Ailion, A. G. Cutillo, A. H. Morris, and K. C. Goodrich, J. Magn. Reson. (1969-1992) **99**, 161 (1992).
[16] A. G. Cutillo, *Application of Magnetic Resonance to the Study of Lung* (Futura, Armonk, NY, 1996).
[17] D. A. Yablonskiy and E. M. Haacke, Magn. Reson. Med. **32**, 749 (1994).
[18] C. H. Ziener, T. Kampf, G. Melkus, V. Herold, T. Weber, G. Reents, P. M. Jakob, and W. R. Bauer, Phys. Rev. E **76**, 031915 (2007).
[19] J. H. Jensen and R. Chandra, Magn. Reson. Med. **44**, 144 (2000).
[20] C. H. Ziener, W. R. Bauer, G. Melkus, T. Weber, V. Herold, and P. M. Jakob, Magn. Reson. Imaging **24**, 1341 (2006).
[21] R. P. Kennan, J. Zhong, and J. C. Gore, Magn. Reson. Med. **31**, 9 (1994).
[22] P. W. Anderson and P. R. Weiss, Rev. Mod. Phys. **25**, 269 (1953).
[23] W. R. Bauer, C. H. Ziener, and P. M. Jakob, Phys. Rev. A **71**, 053412 (2005).
[24] B. Cowan, *Nuclear Magnetic Resonance and Relaxation* (University Press, Cambridge, 1997).
[25] J. H. Jensen, R. Chandra, R. A. Ramani, H. Lu, G. Johnson, S. P. Lee, K. Kaczynski, and J. A. Helpern, Magn. Reson. Med. **55**, 1350 (2006).
[26] H. Cho and Y. Q. Song, Phys. Rev. Lett. **100**, 025501 (2008).
[27] D. S. Grebenkov, Rev. Mod. Phys. **79**, 1077 (2007).
[28] G. Adam and M. Delbrück, in *Structural Chemistry and Molecular Biology*, edited by A. Rich and N. Davidson (Freeman, New York, 1968), pp. 198–215.
[29] H. S. Carslaw and J. C. Jaeger, *Conduction of Heat in Solids* (Clarendon, Oxford, 1959).
[30] A. L. Sukstanskii and D. A. Yablonskiy, J. Magn. Reson. (1969-1992) **167**, 56 (2004).
[31] Y. Ayant, E. Belorizky, J. Alizon, and J. Gallice, J. Phys. (Paris) **36**, 991 (1975).
[32] R. Salomir, B. D. de Senneville, and C. T. W. Moonen, Concepts Magn. Reson., Part B **19B**, 26 (2003).
[33] A. Krogh, J. Physiol. (London) **52**, 409 (1919).
[34] W. R. Bauer and K. Schulten, Magn. Reson. Med. **26**, 16 (1992).
[35] W. Nadler and D. L. Stein, J. Chem. Phys. **104**, 1918 (1996).
[36] A. Szabo, K. Schulten, and Z. Schulten, J. Chem. Phys. **72**, 4350 (1980).
[37] J. R. Reichenbach and E. M. Haacke, NMR Biomed. **14**, 453 (2001).
[38] M. Abramowitz and I. A. Stegun, *Handbook of Mathematical Functions with Formulas, Graphs, and Mathematical Tables* (Dover, New York, 1972).
[39] G. B. Arfken and H. J. Weber, *Mathematical Methods for Physicists* (Elsevier, Oxford, 2005).
[40] L. D. Landau and E. M. Lifshitz, *Course of Theoretical Physics*, 2nd ed. (Pergamon, Oxford, 1999), Vol. 2.
[41] I. S. Gradstein and I. M. Ryshik, *Summen-, Produkt- und Integraltafeln/ Tables of Series, Products, and Integrals* (Deutscher Verlag, Thun, Frankfurt, 1981).
[42] L. P. Hwang and J. H. Freed, J. Chem. Phys. **63**, 4017 (1975).
[43] A. L. Sukstanskii and D. A. Yablonskiy, J. Magn. Reson. **163**, 236 (2003).
[44] K. Schulten, Z. Schulten, and A. Szabo, J. Chem. Phys. **74**, 4426 (1981).
[45] W. Nadler and K. Schulten, J. Chem. Phys. **82**, 151 (1985).
[46] W. Nadler and K. Schulten, J. Chem. Phys. **84**, 4015 (1986).
[47] A. Brünger, R. Peters, and K. Schulten, J. Chem. Phys. **82**, 2147 (1985).
[48] W. B. Jones, W. J. Thron, and H. Waadeland, Trans. Am. Math. Soc. **261**, 503 (1980).
[49] G. Németh, Á. Ág, and G. Páris, J. Math. Phys. **22**, 1192 (1981).
[50] G. A. Baker and P. G. Morris, *Padé Approximants I, II* (Addison-Wesley, Reading, MA, 1981).
[51] J. König, Math. Ann. **23**, 447 (1884).
[52] A. S. Householder, *The Numerical Treatment of a Single Nonlinear Equation* (McGraw-Hill, New York, 1970).
[53] C. W. Gardiner, *Handbook of Stochastic Methods* (Springer, Berlin, 1983).
[54] H. Risken, *The Fokker-Planck Equation* (Springer, Berlin, 1984).
[55] N. G. van Kampen, *Stochastic Processes in Physics and Chemistry* (North-Holland, Amsterdam, 1992).
[56] W. Nadler and D. L. Stein, Proc. Natl. Acad. Sci. U.S.A. **88**, 6750 (1991).
[57] W. R. Bauer and K. Schulten, Ber. Bunsenges. Phys. Chem. **96**, 721 (1992).
[58] I. Oppenheim, K. E. Shuler, and G. H. Weiss, *Stochastic Processes in Chemical Physics* (MIT, Cambridge, 1977).
[59] L. Y. Atanassova, J. Optim. Theory Appl. **84**, 65 (1995).
[60] D. A. Bini, L. Gemignani, and B. Meini, Numer. Math. **89**, 49 (2001).
[61] C. H. Ziener, T. Kampf, G. Melkus, P. M. Jakob, and W. R. Bauer, J. Magn. Reson. **184**, 169 (2007).
[62] S. Wolfram, *The Mathematica Book* (Wolfram Media, Champaign, IL/ Cambridge University Press, Cambridge, 1999).
[63] W. H. Press, S. A. Teukolsky, W. T. Vetterling, and B. P. Flannery, *Numerical Recipes in FORTRAN 77* (Cambridge University Press, Cambridge, 1992).
[64] Wolfram Research, *Mathematica 4.0, Standard Add-On Packages* (Wolfram Media, Champaign, IL/Cambridge University Press, Cambridge, 1999).
[65] A. P. Prudnikov, O. I. Marichev, and Y. A. Brychkov, in *Integrals and Series*, More Special Functions Vol. 3 (Gordon and Breach, New York, 1990).